University
of Glasgow

http://eprints.gla.ac.uk/94707/

Deposited on: 17 July 2014

Monitoring bacterially induced calcite precipitation in porous media using magnetic resonance imaging and flow measurements

E. Sham [a], M.D. Mantle [a], J. Mitchell [a], D.J. Tobler [b], V.R. Phoenix [b], M.L. Johns [c,*]

[a] *Department of Chemical Engineering and Biotechnology, University of Cambridge, Pembroke Street, Cambridge CB2 3RA, UK*
[b] *School of Geographical and Earth Sciences, Gregory Building, University of Glasgow, Glasgow G12 8QQ, UK*
[c] *School of Mechanical and Chemical Engineering, University of Western Australia, 35 Stirling Highway, Crawley, WA 6009, Australia*

ARTICLE INFO

ABSTRACT

A range of nuclear magnetic resonance (NMR) techniques are employed to provide novel, non-invasive measurements of both the structure and transport properties of porous media following a biologically mediated calcite precipitation reaction. Both a model glass bead pack and a sandstone rock core were considered. Structure was probed using magnetic resonance imaging (MRI) via a combination of quantitative one-dimensional profiles and three-dimensional images, applied before and after the formation of calcite in order to characterise the spatial distribution of the precipitate. It was shown through modification and variations of the calcite precipitation treatment that differences in the calcite fill would occur but all methods were successful in partially blocking the different porous media. Precipitation was seen to occur predominantly at the inlet of the bead pack, whereas precipitation occurred almost uniformly along the sandstone core. Transport properties are quantified using pulse field gradient (PFG) NMR measurements which provide probability distributions of molecular displacement over a set observation time (propagators), supplementing conventional permeability measurements. Propagators quantify the local effect of calcite formation on system hydrodynamics and the extent of stagnant region formation. Collectively, the combination of NMR measurements utilised here provides a toolkit for determining the efficacy of a biological–precipitation reaction for partially blocking porous materials.

1. Introduction

Calcite precipitation technology has been used in a wide range of applications including carbon sequestration (Cunningham et al., 2009; Druckenmiller et al., 2006; White et al., 2003), sealing fractured rock (Cunningham et al., 2009; Ferris et al., 1996) and strengthening cracked concrete (De Muynck et al., 2008; Ghosh et al., 2009). Applications specific to contaminant removal include solid-phase capture and remediation of trace metals and radionuclides (Fujita et al., 2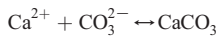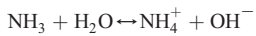004; Warren et al., 2001), and treatment of calcium in wastewaters (Hammes et al., 2003). Calcite precipitation can occur naturally in sediments and reservoirs (Kralj and Vdović, 2000) and can also be forced to occur under certain conditions, for example fillers in industrial products (Renaudin et al., 2008).

Calcite precipitation can be induced bacterially using *Sporosarcina pasteurii* (formally *Bacillus pasteurii*) via ureolysis. During ureolysis, bacteria use urea as a nitrogen and energy source and hydrolyse it to form ammonia and by-products consisting of carbonates and bicarbonates. This process raises the alkalinity of the solution, creating an alkaline environment in which calcium carbonate precipitation becomes favourable (Chou et al., 2008) by the following series of reactions:

$$NH_2CONH_2 + 2H_2O \rightarrow 2NH_3 + HCO_3^- + H^+$$
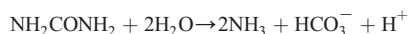
* Corresponding author. Tel.: +61 8 6488 5664.
 E-mail address: michael.johns@uwa.edu.au (M.L. Johns).

$$NH_3 + H_2O \leftrightarrow NH_4^+ + OH^-$$

$$HCO_3^- + H^+ + 2OH^- \leftrightarrow CO_3^{2-} + 2H_2O$$

$$Ca^{2+} + CO_3^{2-} \leftrightarrow CaCO_3$$

Laboratory studies have extensively demonstrated the use of ureolysis-driven calcite precipitation by *S. pasteurii* to reduce the porosity and hence the permeability of sand columns (e.g. Cunningham et al., 2009, 2011; DeJong et al., 2006; Ferris et al., 1996; Gollapudi et al., 1995; Harkes et al., 2010; Tobler et al., 2012; Whiffin et al., 2007). Optimum injection strategies have been studied (Ebigbo et al., 2012; Tobler et al., 2012) and the morphology of the carbonate precipitates quantified as a function of various process conditions (Cuthbert et al., 2012). Collectively, all such studies have relied on macroscopic measurements of the sample effluent or detailed analysis following destructive sampling. In the current study we employ a suite of non-invasive nuclear magnetic resonance (NMR) techniques to quantify the effect of calcite precipitation on spatial porosity distribution and transport processes. The former is probed via the application of multi-dimensional magnetic resonance imaging (MRI); the latter via NMR pulsed field gradient (PFG) measurements. NMR PFG is able to produce propagators, which are probability distributions of displacement over a given observation time (Δ). Both a model glass bead random packing and a sandstone rock core are considered as the sample porous media. All the NMR measurements utilised here are sensitive to the protons (^{1}H) in the aqueous fluid-phase allowing the water transport through the heterogeneous pore structure to be monitored exclusively as the calcite formation progresses.

2. Background

2.1. NMR applied to calcite precipitation

Previous use of NMR techniques, similar to the one we employ here to study calcite precipitation in porous media, is limited to Fridjonsson et al. (2011). They investigated calcite precipitation via *S. pasteurii* in a model porous system consisting of 241 μm diameter monodisperse polystyrene beads packed randomly in a 10 mm internal diameter cylindrical column. Changes in the pore space distribution following calcite precipitation were revealed via both MRI and, at the pore scale, by light microscopy following destructive sampling. The effect of inoculation was evident in displacement propagator measurements which indicated increased pore-scale mixing, a reduction in effective stagnant zones, and effectively a more homogeneous pore space.

More conventional use of NMR techniques to investigate calcite precipitation is frequent in the literature. For example, NMR spectroscopy has been used to test whether non-enzymatic protein of the pancreatic juice can inhibit calcium carbonate precipitation inside the body as this can lead to stones forming in the pancreatic ducts (Reggi et al., 1998). It has also shown that dissolved organic ligands can interact strongly with a calcite surface (Phillips et al., 2005). The detailed structural analysis of extensive precipitation of calcite on glasses has also been made using magic angle spinning (MAS) NMR in conjunction with infrared spectroscopy (FTIR) and Raman measurements (Kansal

et al., 2011). These combined techniques were used to look at the surface of precipitated calcite particles modified by the reaction of phosphonic acids in organic solvents, tetrahydrofuran (THF) and ethanol (Malti et al., 2012). Paper coating layers with a porous structure that had various amounts of kaolin and precipitated calcium carbonate pigments were studied using PFG NMR measurements of restricted water diffusion absorbed in the coatings (Li et al., 1999).

2.2. Propagator measurements

Tracer tests are typically used to investigate subsurface regions and take many forms with the characterisation relating to the number and types of tracers used (Shook et al., 2004). For example, a radioactive tracer was used to evaluate the subsurface water and contaminant transport processes in a heterogeneous field-scale system (Dunnivant et al., 1998) whilst a two forced-gradient, recirculating-loop tracer experiment was conducted to assess the feasibility of encapsulated cell transport and bioremediation on the basis of polystyrene microsphere transport results (Petrich et al., 1998). Experimental tracer breakthrough curves have also been compared with modelled data which have allowed for improved representations of the heterogeneity in a 3D aquifer flow model (e.g. Devlin et al., 2012).

PFG NMR probability distributions of molecular displacement (flow propagators) provide a method of characterising fluid flow through a porous system. The measured displacements are averaged across the sample over a defined observation time. Propagators are akin to in situ tracer methods, except the NMR measurement tracks the species of interest directly (in this case water) without the need to inject tracer particles. The inclusion of spatial selectivity in the PFG methodology allows entry and exit effects in short samples to be removed (Hussain et al., 2011).

PFG NMR techniques were originally developed by Stejskal and Tanner (1965) and are used to measure molecular self diffusion and advection. The technique has since been modified to reduce the adverse effect of additional magnetic field gradients due to susceptibility contrast (e.g., Cotts et al., 1989), to reduce the influence of relaxation weightings (Mitchell et al., 2008b; Scheven et al., 2005b) and also to rapidly acquire multiple flow propagators (Mitchell and Johns, 2009). Previously, flow propagator measurements have been used to study the Stokes' flow regime in opaque porous systems, specifically glass bead packs and rock cores (e.g., Mitchell et al., 2008a,b; Scheven et al., 2005a), and used to monitor, for example, the effect of biofilm growth (Seymour et al., 2004; von der Schulenburg et al., 2008). Research has also been conducted using propagators in systems with multiphase flow (e.g., Tessier and Packer, 1998) and colloidal transport through porous media (Creber et al., 2009). By comparing displacement propagators before and after pore space modification, structural changes in porous media are observed, such as permeability changes due to polymer treatment in reservoir rocks (Johns et al., 2003).

3. Materials and methods

Two porous media supports were considered: glass beads (randomly packed) and Bentheimer sandstone rock core (containing little clay). In terms of basic characterisation of

these systems: permeability was measured using a deionised water flow from 10 to 45 ml min^{-1}. The permeability (κ) was determined using Darcy's law:

$$\kappa = \frac{\mu \Delta x}{\Delta P} v, \tag{1}$$

where μ is viscosity, Δx is the length of the bed, v is the flowrate and ΔP is the pressure drop across the bed. Bypassing of the bead packs along the wall was minimised as the column-to-bead diameter ratio is 370:1, in excess of the recommended ratio of 10:1 (Sederman et al., 2001), whilst for the rock cores the pressure on the confining sleeve was ensured to exceed the operating pressure by at least an order of magnitude. Porosity values were determined by gravimetrically determining the mass of water in the samples.

3.1. Blocking of bead pack

The model porous medium consisted of 100 ± 20 μm borosilicate ballotini (sourced from Q.A. Equipment Ltd., UK) packed randomly in a cylindrical Perspex column of length 105 mm and internal diameter 37 mm. A sintered glass disc (100–160 μm pore size) was placed at the bottom of the column to aid fluid distribution within the column, and to contain the beads and allow the solutions to flow freely. The column was packed under water and a tapping motion was used to dislodge any air bubbles. The packing porosity (σ), with no calcite precipitation, was determined gravimetrically to be $\sigma = 0.385 \pm 5 \times 10^{-3}$. The unfouled permeability was determined to be $\kappa = 8.44$ μm^2.

A suspension of the urease positive strain *S. pasteurii* at an optical density (OD) of 0.15 in deionised water (DW) was prepared and pH adjusted as described by Tobler et al. (2011). A staged injection approach was chosen where *S. pasteurii* was first injected (vertical flow) for approximately 2 h, ensuring that equilibrium was achieved between the suspended and adsorbed *S. pasteurii* cells and that all natant liquid has been flushed out. The bead column was then left static (no flow) for 2 h to allow the microbes to attach to the beads. During the second stage, the cementation fluid containing 50 mM CaCl$_2$ and 50 mM urea was pumped continuously for 2 days until a new batch of bacteria was injected into the columns and the cycle repeated. The flow rate was 1 ml min^{-1}. The changes in the head gradient across the column were measured over time and the experiment was stopped once a backpressure of approximately 1.93×10^4 Pa (equivalent to a hydraulic head of 2 m) was reached. NMR measurements were carried out before fouling (unfouled) and after 4 (fouled once) and 9 (fouled twice) bacterial injection cycles respectively. A cycle refers to the staged injection approach outlined above; for clarity we note that this consists of a 2 hour *S. pasteurii* cell injection followed by a 2 day injection of cementation fluid.

3.2. Blocking of sandstone rock core

Pore space plugging within a Bentheimer sandstone rock core-plug (external dimensions: 70.5 mm length, 37 mm diameter) was investigated using a high-pressure system. The system consisted of two high pressure isocratic pumps and a stainless steel core holder (TEMCO Inc., Tulsa, OK). The core holder was connected to a back pressure regulator via a

double valve to obtain a confining pressure of 1.72×10^6 Pa on the core. Prior to loading, the sandstone core was washed and saturated with deionised water. The porosity of the sandstone core was $\sigma = 0.231$ as determined gravimetrically. The permeability of the unfouled sandstone core was determined to be $\kappa = 1.01$ μm^2.

Similar to the bead pack experiment, a staged injection approach was chosen for the sandstone experiment. First, a suspension of *S. pasteurii* (in DW) at an OD of 0.45 was injected for 2 h, followed by a static period of 2 h for bacterial attachment. During the second stage, the cementation fluid containing 1 M CaCl$_2$ and 1 M urea was injected for approximately 1 h before the flow was stopped. The fluid in the rock core was allowed to react for a day under static conditions, before the core was flushed with DW and amended with new bacteria the following day. Note that once the backpressure reached 2.07×10^4 Pa, the injected bacterial density was lowered to 0.15 to avoid plugging by biomass. The injection flow rate was 1 ml min^{-1}. The filling procedure was stopped once a backpressure of 3.86×10^5 Pa was reached (after 22 bacterial injections). NMR measurements were carried out before fouling (unfouled) and after 13 (fouled once) and 22 (fouled twice) bacterial injection cycles.

3.3. NMR measurements of bead pack column and sandstone core

For NMR measurements, the sandstone was mounted in a polyether ether ketone (PEEK) core holder (purchased from Ergotech Ltd., Conway, UK). A confining pressure of 2.5×10^6 Pa was applied using a per-fluorinated oil (Fluorinert FC-43), ensuring no background NMR signal was obtained from the core holder. Distributor plates were used on either end of the respective samples, these were checked at the end of the experiments for any calcite precipitation; none was found. Continuous flow of deionised water through the porous media was achieved using a Teledyne ISCO model 260D syringe pump. Pressure measurements with deionised water were used to determine the permeability of the samples by fitting a linear trend line to variation in pressure drop with flow rate. Eq. (1) shows Darcy's Law, the relationship linking the viscosity μ, length of the bed Δx, flow rate v, and the pressure drop ΔP to the permeability κ.

All NMR measurements were performed on a horizontal-bore Bruker AV 85 magnet with a magnetic field strength of 2 T, corresponding to a resonant frequency of 85.18 MHz for ^{1}H detection (which was exclusively used in our experiments). Radio frequency (rf) excitation and detection were achieved with a birdcage resonator (60 mm inner diameter). Rf pulse durations of $t_{90} = 15$ μs and $t_{180} = 30$ μs, corresponding to tip angles of 90° and 180°, respectively, were used in all the NMR experiments. NMR characterisation of the porous media consisted of measurements of longitudinal T_1 and transverse T_2 relaxation times, 1D profiles, and 3D images. Flow propagators, acquired using NMR PFG, were then measured across a range of flow rates and observation times. This collective experimental NMR suite was applied to the untreated porous media samples (model glass bead packings and sandstone rock cores), and following both the single and repeated calcite precipitation treatment (i.e., fouled once and fouled twice respectively), as described above.

The T_1 relaxation time was determined using the standard inversion-recovery sequence (Vold et al., 1968) and the T_2 relaxation time was determined using the standard Carr–Purcell Meiboom–Gill sequence (Carr and Purcell, 1954; Meiboom and Gill, 1958) with $n = 8$ echoes and an echo time of $t_E = 5$ ms. Spin echo 1D profiles (Callaghan, 1991) were acquired along the axis of the cylindrical sample (z-axis) with 128 pixels and a field of view of 150 mm, giving a spatial resolution of $\Delta z = 1.17$ mm. The echo time was $t_E = 5.23$ ms and the repetition time was $t_R = 30$ s, sufficient to effectively ensure full signal recovery. Spin echo 3D images were also acquired, with an effective cubic voxel size of 625 μm × 625 μm × 625 μm. The average relaxation times for the unfouled bead pack and sandstone were $T_1 = 1.51$ s and $T_2 = 123$ ms and $T_1 = 1.28$ s and $T_2 = 100$ ms respectively. These reduced as follows for the fouled twice measurements: $T_1 = 1.47$ s and $T_2 = 107$ ms and $T_1 = 1.18$ s and $T_2 = 72$ ms for the bead pack and sandstone respectively. Longitudinal (T_1) relaxation losses were effectively eliminated through the use of sufficiently long repetition times (t_R). Transverse (T_2) relaxation losses were deemed to be negligible at consistently less than 4%. To quantify the MRI signal intensity, a calibration phantom was constructed by mixing normal (deionised) water with heavy water (D_2O, Aldrich 99%) such that the volumetric H_2O fraction was 0.3. The profiles and images obtained from this phantom were used to calculate a calibration factor so that the NMR images, being a measure of magnetization [arbitrary units], were rescaled to a quantitative volumetric liquid fraction.

The flow propagators were acquired using a modified version of the alternating pulsed gradient stimulated echo (APGSTE) sequence, Fig. 1, based on the 13-interval Cotts sequence (Cotts et al., 1989). The modification incorporates a spatially selective soft 180° rf pulse, allowing signal to be acquired from a central portion of the sample (Hussain et al., 2011) to avoid entrance/exit effects — signal was acquired from slices of thickness 18.8 mm, centred at a position of 52.5 mm along the bead pack of total length 105 mm for the bead pack. For the sandstone rock core, slices 18.3 mm thick were taken from the same location at the centre of the rock core, located 35.3 mm along the total sample length of 70.5 mm. A Gaussian rf pulse with duration, 256 μs, corresponding to the 180° tip angle at a gradient strength $g = 10$ G cm^{-1} was used for the slice selections. Propagators were acquired over a range of gradient strengths $g = -10$ to 10 G cm^{-1} with 33 equidistant q-space points (where q is the Fourier reciprocal of displacement: $q = \gamma g \delta / 2\pi$). Observation

times of $\Delta = 100, 500, 1000,$ and 2000 ms were used, following the definition of Δ given in Cotts et al. (1989). For the bead pack, volumetric flow rates of $Q = 0.5$ and 1 ml min^{-1} were used and for the sandstone, flow rates of $Q = 7, 15, 20,$ and 25 ml min^{-1} were used. To prevent aliasing in q-space over the range of Δ and Q, the bipolar gradient pulse duration was varied from $\delta = 0.41$ to 4.5 ms.

4. Results and discussion

4.1. Bead pack

The porosity of the bead pack is defined as the ratio of pore volume to total sample volume. The porosity, determined gravimetrically, was seen to reduce from $\sigma = 0.385 \pm 0.005$ to 0.357 ± 0.005 (a 7% reduction in pore volume) following the first set of treatments (fouled once). The porosity was then further reduced to $\sigma = 0.348 \pm 0.05$ during the second set of treatments (fouled twice), corresponding to a 9.6% reduction in pore volume relative to the non-fouled bead pack. The permeability was also found to have decreased from $\kappa = 8.44$ μm^2 to 5.9 μm^2, and then finally to $\kappa = 0.1$ μm^2 after the two fouling treatments (fouled once and fouled twice), respectively.

Fig. 2 shows quantitative porosity profiles along the length of the bead pack. The average porosity (as calculated via averaging of the values along the profile) is seen to reduce from $\sigma = 0.345 \pm 0.006$ to 0.310 ± 0.006 to 0.295 ± 0.006 respectively, following the two fouling treatments. The resultant % reduction is consistent with the gravimetric measurements; the systematic difference we attribute to the presence of gas bubbles which result in an underestimation of porosity for the NMR measurements and an overestimation of porosity in the case of the gravimetric measurement. In Fig. 2, the calcite can be seen to have formed along the sample length with predominately more precipitate formation at the entrance. Despite the relatively modest reductions in average porosity, we observe substantial reductions in permeability (almost two orders in magnitude following the second treatment) indicating that the inlet region of greatest porosity reduction is almost impermeable following the second set of treatments. We also
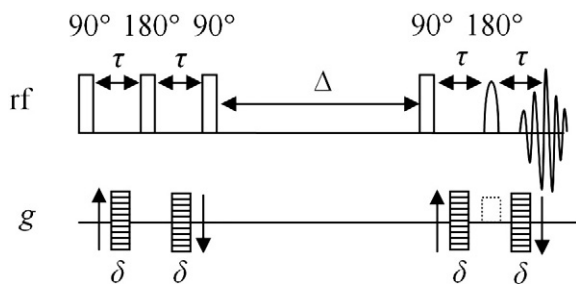

Fig. 1. Modified APGSTE pulse sequence with a truncated Gaussian 180° soft rf pulse used for slice-selective signal acquisition. The observation time, bipolar gradient pulse duration and time between the applications of the rf pulses have been denoted with Δ, δ and τ respectively.
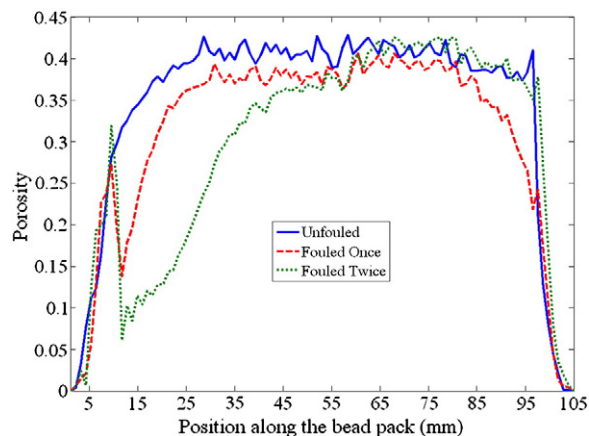

Fig. 2. Variation in porosity of the bead pack during the fouling sessions. The bead pack inlet starts at 0 mm with the outlet at 105 mm. The direction of flow is left to right in the figure.

note an increase in porosity towards the exit of the packing between the fouled once and fouled twice measurements — this must indicate detachment of calcite precipitates in this region between these two measurements.

Fig. 3 shows nine quantitative 2D cross-sectional slices from 3D images of the local porosity at distances 15, 65 and 95 mm from the inlet for the unfouled, fouled once and fouled twice bead packs. The images have an in-plane resolution of 625 μm × 625 μm and slice thickness of 625 μm. The images show that the precipitate has successfully blocked the entrance (15 mm from inlet), substantially reducing the local porosity in the inlet as discussed above — the porosity in this slice is reduced from 0.352 to 0.255 to 0.104 following the two fouling treatments. The gas bubbles mentioned above are evident in the image as small black regions surrounded by local bright rings. This is a characteristic feature of such bubbles and results from magnetic field distortions due to local susceptibility contrast between the gas and liquid. The preferential precipitation of calcite near the entrance of our sample is in contrast to the more heterogeneous dendritic pattern observed in Fridjonsson et al. (2011); this is perhaps not surprising given the significantly different calcite precipitation procedures employed, notably the following: we employ 100 μm diameter ballotini in a 37 mm inner diameter column versus 241 μm diameter ballotini in a 10 mm inner diameter column; we employ concentrations of $CaCl_2$ and Urea of 5.5 and 3 g l^{-1} versus 20 g l^{-1} and 3.7 g l^{-1}. Most importantly we subject our packing to between 4 and 9 cycles of S. pasteurii injection (for 2 h) followed by 2 h of cementation fluid injection; in Fridjonsson et al. (2011) 6.5 ml of a S. pasteurii solution was injected followed by exposure to a nutrient medium for 1 h at 10 ml hr^{-1} (followed by 10 minute exposure to a Ca containing nutrient solution). Fridjonsson et al. (2011) also applied a nutrient broth between NMR experiments to sustain biological growth whereas we did not.

Fig. 4 shows the slice propagators of thickness 18.8 mm acquired for the bead pack at an observation time of 1 s for a flowrate of 0.5 ml min^{-1}. The slices were taken centred at a position of 52.5 mm along the bead pack of total length 105 mm (Fig. 2). Minimal differences are evident. This is expected given that the local porosity (as extracted from Fig. 2) for the respective slice is observed to decrease only from $\sigma = 0.409$ to 0.382, and then to $\sigma = 0.374$ for the unfouled, fouled once and fouled twice measurements, respectively. Propagators were not acquired closer to the inlet (which displayed a greater reduction in porosity as discussed above), as they would be distorted by entrance effects caused by the distributor plates.

4.2. Sandstone

The porosity of the Bentheimer sandstone was seen to decrease from $\sigma = 0.231$ to 0.177 (23% reduction in pore volume), and then $\sigma = 0.159$ (further 10% reduction) after the first and second fouling, as determined gravimetrically. The permeability for the unfouled Bentheimer sandstone was found to be $\kappa = 1.01$ μm^2 which is consistent with the range of 1–2 μm^2 typically reported in the literature (Dautriat et al., 2009; Verganelakis et al., 2005). After the first and second fouling sessions the permeability was found to have decreased to $\kappa = 0.705$ μm^2 and 0.035 μm^2, respectively, indicating a
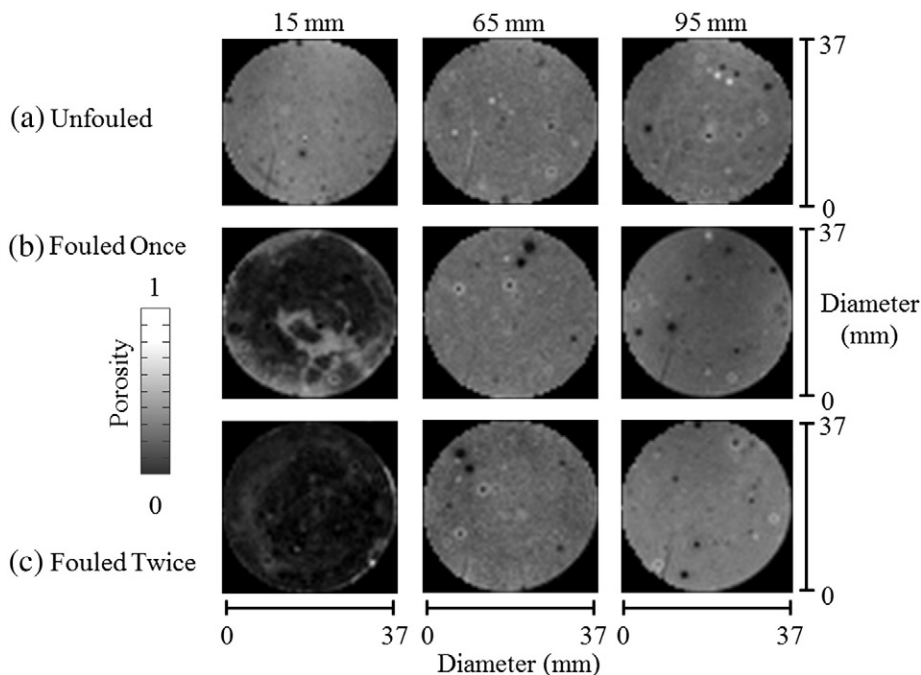

Fig. 3. Nine two-dimensional slices in the horizontal plane taken from a three-dimensional image of the local porosity at slices centred 15, 65 and 95 mm beyond the inlet face of (a) the non-fouled bead pack (0 injection cycle), (b) the bead pack fouled once (4 injection cycles), and (c) the bead pack fouled twice (9 injection cycles). The images have an in-plane resolution of 625 μm by 625 μm and slice thickness of 625 μm. The average porosities are: (a) 32, 0.41 and 0.38; (b) 0.2, 0.37 and 0.29 and (c) 0.08, 0.37 and 0.36 respectively.
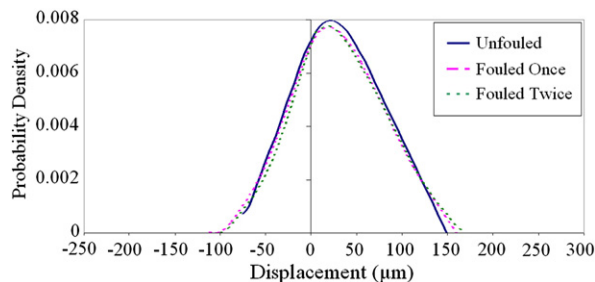
Fig. 4. The differences between the fouled and non-fouled displacement propagators for the bead packing at 0.5 ml min^{-1} at an observation time of 1 s. The acquisition slice of thickness 18.8 mm was acquired at 52.5 mm from the inlet to the packing.

more impervious system. By providing an overall permeability reduction of 96.5%, the calcite precipitate has proven itself to be a very effective tool for reducing permeability in this sandstone formation. The final porosity of 0.159 corresponds to a 96.5% reduction in permeability relative to the initial porosity of 0.231. However between the first and second fouling, a reduction in porosity of only 0.018 resulted in a permeability reduction of 95% suggesting the system is near its percolation threshold (at which point the permeability would be effectively zero). There are probably only a few active flow channels in the core after the second fouling period, this will be explored further below with respect to the displacement propagator data acquired for this system. It is also plausible that local mass transfer limitations are operational resulting in preferential calcite precipitation in comparatively larger pores (particularly during the second fouling period) compared to smaller pores (less accessible and hence more mass transfer limited) and a consequential enhanced reduction in system permeability (which is preferentially dictated by the larger pores).

Fig. 5 shows the quantitative porosity profiles along the length of the sandstone, the calcite is seen to have formed more evenly along the length of the core-plug compared to the bead packs (cf. Fig. 2), no significant porosity variation is evident
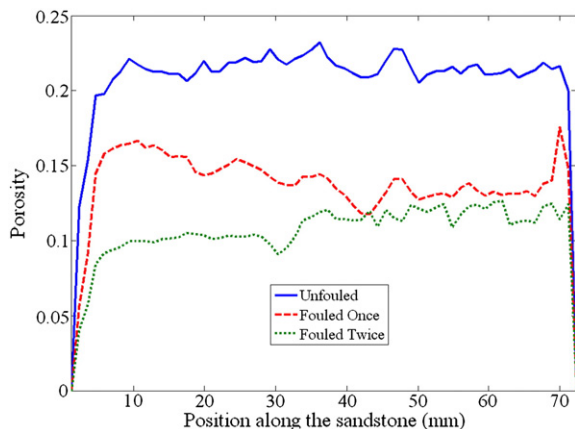

Fig. 5. Variation in porosity of the sandstone core during the fouling sessions. The direction of flow is from left to right in the figure.

in either the radial or the two Cartesian directions presented. The average initial porosity for the column was determined from the 1D profile in Fig. 5 to be $\sigma = 0.205 \pm 0.006$. The average porosities after the first and second fouling were $\sigma = 0.135 \pm 5.76 \times 10^{-3}$ and $0.105 \pm 5.76 \times 10^{-3}$, respectively. This trend is again consistent with the gravimetric measurements; and the systematic difference is again attributed to the presence of gas bubbles. The second fouling resulted in a modest decrease in porosity but a substantial decrease (20 fold) in permeability. Fig. 6 shows nine quantitative 2D x–y slices from a 3D image of the local porosity at distances 10, 30 and 60 mm from the inlet of the sandstone rock core. The images have an in-plane resolution of 625 μm × 625 μm and slice thickness of 625 μm. The images agree with the 1D profiles in that they show uniform calcite deposition along the column length. However, also evident is the relatively homogeneous calcite precipitation across the core-plug cross-section. As noted by Fridjonsson et al. (2011), the limited spatial resolution of MRI prevents observation of pore-scale events — the resolution of 625 μm in our images means that each voxel contains ~1000 pores, given a typical pore diameter of 45 μm (Mitchell et al., 2010). Comparison between the bead packs and the sandstone is difficult as different conditions (most notably cell suspension density and CaCl$_2$) were used during biofilm growth and calcite precipitation. However what is immediately obvious is the greater, more homogeneous deposition of calcite in the sandstone cores relative to the bead packs. In addition, a 3.7% reduction in absolute porosity in the bead packs resulted in a 98% reduction in permeability, whereas a 7.2% reduction in absolute porosity in the sandstone cores resulted in only a 96.5% reduction in permeability. This we speculate to be a consequence of the greater calcite precipitation near the entrance of the bead packs. We re-iterate that different conditions were employed with respect to the sandstone and the bead packs and that any further comparisons should be made with caution. It is also plausible that local mass transfer limitations are operational resulting in preferential calcite precipitation in comparatively larger pores (particularly during the second fouling period) compared to smaller pores and a consequential enhanced reduction in system permeability.

Fig. 7 shows the slice propagators of thickness 18.3 mm taken from the sandstone at 7, 15, 20 and 25 ml min^{-1} at an observation time of 1 s. All the slices were taken at the same location centrally at a position of 35.3 mm along the sandstone core of total length 70.5 mm (Fig. 5). Ca analysis of the effluent and the reproducibility of the propagators acquired at the higher flowrates indicated that the calcite was able to attach firmly in place and not be flushed out. The local porosities at the corresponding relative slice in the 1D profiles were determined to be $\sigma = 0.219$, 0.135, and 0.110 for the unfouled, fouled once, and fouled twice measurements, respectively. Using the mean displacement, as determined from the propagators in Fig. 7, equivalent porosities were determined; these agreed with the profile measurements to within 12%. Such differences are the consequence of signal relaxation during propagator acquisition due to both surface relaxation and transport through susceptibility gradients, as discussed in detail by Scheven et al. (2005a,b). Fig. 7(a) shows the mean displacement increasing with increasing flow rate as expected for the unfouled sandstone. In comparison, the
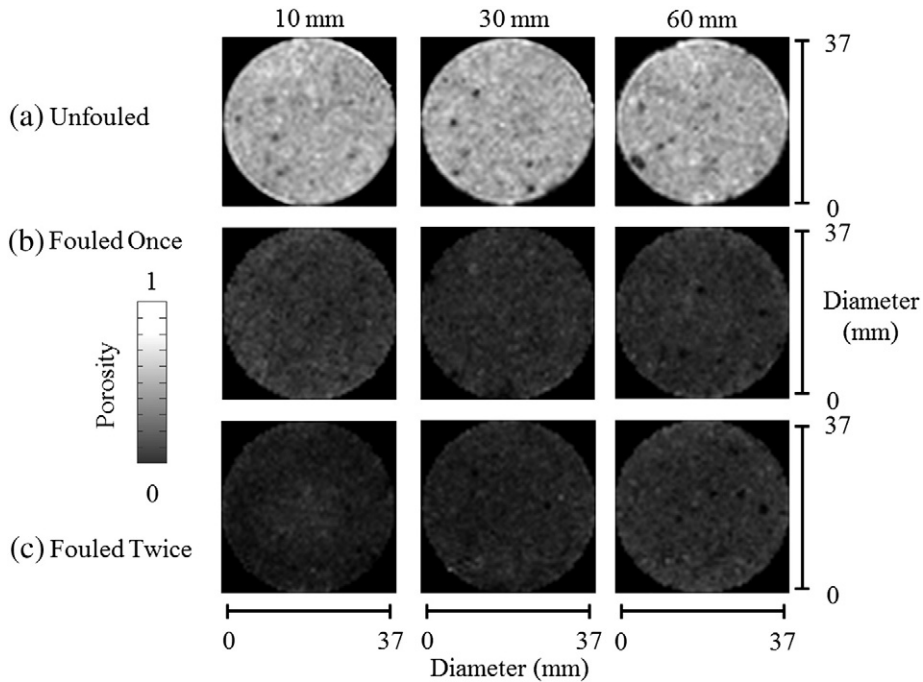
Fig. 6. Nine two-dimensional slices in the horizontal plane taken from a three-dimensional image of the local porosity at slices centred 10, 30 and 60 mm beyond the inlet face of (a) the non-fouled sandstone core (0 injection cycle), (b) the sandstone core fouled once (13 injection cycles), and (c) the sandstone core fouled twice (22 injection cycles). The images have an in-plane resolution of 625 μm by 625 μm and slice thickness of 625 μm. The average porosities are: (a) 0.22, 0.23 and 0.21; (b) 0.16, 0.14 and 0.1 and (c) 0.09, 0.1 and 0.13 respectively.

propagators obtained in the fouled rock, Fig. 7(b) and (c), have two main differences: (1) the stagnant peak is much more prominent, and (2) significantly larger displacements are observed. The transformation in the propagators shows that the calcite formation is changing the flow paths in the sandstone and increasing its heterogeneity (e.g., an increase in the number of dead-end pores). Significant regions of stagnation are being created whilst significant flow channels are experiencing considerably larger velocities. Interestingly this increase in heterogeneity is the reverse of what was observed in the propagators acquired by Fridjonsson et al. (2011) for fouled bead packs, where more homogeneity (reduced stagnant zones)
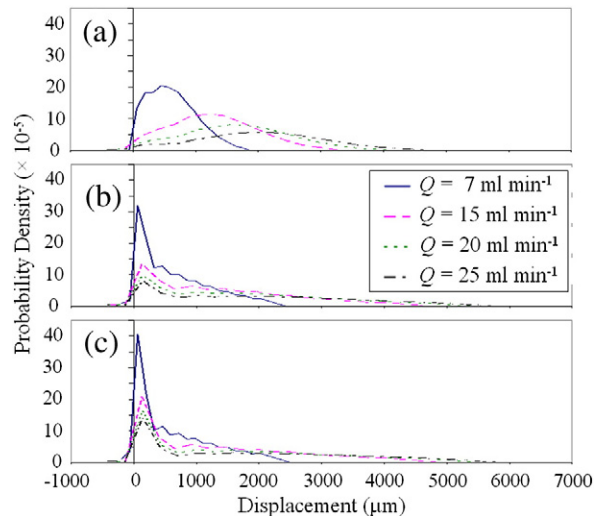

Fig. 7. Slice displacement propagators for the (a) non-fouled (b) fouled once and (c) fouled twice sandstone cores with Q = [7, 15, 20, 25] ml min^{-1}, Δ = 1 s. The slices of thickness 18.3 mm were acquired 35.3 mm from the inlet to the core.

was clearly evident as fouling progressed; however, as noted in Section 3, there are considerable differences in the calcite precipitation procedures.

5. Conclusions

Non-invasive measurements of liquid flow by nuclear magnetic resonance (NMR) are made in a model porous system and a sandstone core-plug before and after a biologically mediated calcite precipitation reaction. Standard magnetic resonance imaging (MRI) techniques were used to acquire 1D and 3D porosity maps before and after precipitation. These images allowed the identification of the spatial distribution of calcite precipitation. Different filling injections were used to significantly reduce the permeability of the bead pack and sandstone cores due to their different heterogeneities and internal structures. Very homogeneous (within the spatial resolution limits of the 3D MRI technique) calcite precipitation was observed in the sandstone rock core with a modest reduction in overall porosity but a substantial reduction in permeability; this we attribute to the system approaching its percolation threshold and/or mass transfer limitations resulting in preferential deposition in larger pores (this would be considerably below the 0.5 mm resolution of the MRI measurements). We note that the MRI techniques we employ probe porosity variations at a resolution in excess of the pore size; if pore size distributions are required these can be accessed using X-ray micro-tomography or mercury porosimetry. However, we note that these are both incompatible with repeated measurements on the same bacterial-containing sample. In future we will employ NMR T_2 distribution measurements as a method of measuring the changing pore size distributions of the samples following calcite precipitation.

For the bead packs, preferential precipitation was observed near the entrance with a substantial reduction in permeability following a second calcite precipitation treatment. Displacement propagators for the sandstone revealed a significantly more heterogeneous pore space with significant stagnant regions and enhanced flow channels. The NMR/MRI data was shown to complement permeability and gravimetric porosity tests to characterise and understand where the calcite had formed and its effect on the hydrodynamics of fluid moving in the pore network.

The use of such calcite precipitate to seal fractured rock systems is arguably of greater practical importance. Preliminary results have indicated that 2D MRI velocimetry is very sensitive to the effect of calcite precipitation in artificially fractured rock cores. This will be explored in much greater depth in future using a wider range of NMR measurements, rock types and fracture techniques. The NMR/MRI data will also be used to validate models of the calcite precipitation. Collectively, these measurements will be used to optimise calcite precipitation techniques in terms of permeability reduction in both fractured and un-fractured formations.

Acknowledgements

References

Callaghan, P.T., 1991. Principles of Nuclear Magnetic Resonance Spectroscopy. Oxford University Press, UK.

Carr, H.Y., Purcell, E.M., 1954. Effects of diffusion on free precession in nuclear magnetic resonance experiments. Physical Review 94 (3), 630–638.

Chou, C.W., Seagren, E., Aydilek, A., 2008. Bacterially-induced calcite precipitation via ureolysis. [Online] Available from: http://www.microbelibrary.org/library/laboratory-test/3174-bacterially-induced-calcite-precipitation-via-ureolysis.

Cotts, R.M., Hoch, M.J.R., Sun, T., Markert, J.T., 1989. Pulsed field gradient stimulated echo methods for improved NMR diffusion measurements in heterogeneous systems. Journal of Magnetic Resonance 83 (2), 252–266.

Creber, S.A., Pintelon, T.R.R., Johns, M.L., 2009. Quantification of the velocity acceleration factor for colloidal transport in porous media using NMR. Journal of Colloid and Interface Science 339, 168–174.

Cunningham, A.B., Gerlach, R., Spangler, L., Mitchell, A.C., 2009. Microbially enhanced geologic containment of sequestered supercritical CO_2. Energy Procedia 1, 3245–3252.

Cunningham, A.B., Gerlach, R., Spangler, L., Mitchell, A.C., Parks, S., Phillips, A., 2011. Reducing the risk of well bore leakage of CO_2 using engineered biomineralization barriers. Energy Procedia 4, 5178–5185.

Cuthbert, M.O., Riley, M.S., Handley-Sidhu, S., Renshaw, J.C., Tobler, D.J., Phoenix, V.R., Mackay, R., 2012. Controls on the rate of ureolysis and the morphology of carbonate precipitated by *S. pasteurii* biofilms and limits due to bacterial encapsulation. Ecological Engineering 41, 32–40.

Dautriat, J., Gland, N., Guelard, J., Dimanov, A., Raphanel, J.L., 2009. Axial and radial permeability evolutions of compressed sandstones: end effects and shear-band induced permeability anisotropy. Pure and Applied Geophysics 166, 1037–1061.

De Muynck, W., Debrouwer, D., De Belie, N., Verstraete, W., 2008. Bacterial carbonate precipitation improves the durability of cementitious materials. Cement and Concrete Composites 38, 1005–1014.

DeJong, J.T., Fritzges, M.B., Nüsslein, K., 2006. Microbially induced cementation to control sand response to undrained shear. Journal of Geotechnical and Geoenvironmental Engineering 132, 1381–1392.

Devlin, J.F., Schillig, P.C., Bowen, I., Critchley, C.E., Rudolph, D.L., Thomson, N.R., Tsoflias, G.P., Roberts, J.A., 2012. Applications and implications of direct groundwater velocity measurement at the centimetre scale. Journal of Contaminant Hydrology 127, 3–14.

Druckenmiller, M.L., Maroto-Valer, M.M., Hill, M., 2006. Investigation of carbon sequestration via induced calcite formation in natural gas well brine. Energy & Fuels 20, 172–179.

Dunnivant, F.M., Newmann, M.E., Bishop, C.W., Burgess, D., Giles, J.R., Higgs, B.D., Hubbell, J.M., Neher, E., Norrell, G.T., Pfiefer, M.C., Porro, I., Starr, R.C., Wylie, A.H., 1998. Water and radioactive tracer flow in a heterogeneous field-scale system. Ground Water 36 (6), 949–958.

Ebigbo, A., Phillips, A., Gerlach, R., Helmig, R., Cunningham, A.B., Class, H., Spangler, L., 2012. Darcy-scale modeling of microbially induced carbonate mineral precipitation in sand columns. Water Resources Research 48, W07519.

Ferris, F.G., Stehmeier, L.G., Kantzas, A., Mourits, F.M., 1996. Bacteriogenic mineral plugging. Journal of Canadian Petroleum Technology 36 (9), 56–61.

Fridjonsson, E.O., Seymour, J.D., Schultz, L.N., Gerlach, R., Cunningham, A.B., Codd, S.L., 2011. NMR measurement of hydrodynamic dispersion in porous media subject to biofilm mediated precipitation reactions. Journal of Contaminant Hydrology 120–121, 79–88.

Fujita, Y., Redden, G.D., Ingram, J.C., Cortez, M.M., Ferris, F.G., Smith, R.W., 2004. Strontium incorporation into calcite generated by bacterial ureolysis. Meeting on Microbial Geochemistry Held at the 2002 Fall Meeting of the AGU, San Francisco, CA, pp. 3261–3270.

Ghosh, S., Biswas, M., Chattopadhyay, B.D., Mandal, S., 2009. Microbial activity on the microstructure of bacteria modified mortar. Cement and Concrete Composites 31, 93–98.

Gollapudi, U.K., Knutson, C.L., Bang, S.S., Islam, M.R., 1995. A new method for controlling leaching through permeable channels. Journal of Chemosphere 30 (4), 695–705.

Hammes, F., Seka, A., Van Hege, K., Van De Wiele, T., Vanderdeelen, J., Siciliano, S.D., Verstraete, W., 2003. Calcium removal from industrial wastewater by bio-catalytic $CaCO_3$ precipitation. Journal of Chemical Technology and Biotechnology 78, 670–677.

Harkes, M.P., van Paassen, L.A., Booster, J.L., Whiffin, V.S., van Loosdrecht, M.C.M., 2010. Fixation and distribution of bacterial activity in sand to

induce carbonate precipitation for ground reinforcement. Ecological Engineering 36, 112–117.

Hussain, R., Pintelon, T.R.R., Mitchell, J., Johns, M.L., 2011. Using NMR displacement measurements to probe CO_2 entrapment in porous media. AIChE Journal 57 (7), 1700–1709.

Johns, M.L., Sederman, A.J., Gladden, L.F., Wilson, A., Davies, S., 2003. Using MR techniques to probe permeability reduction in rock cores. AICHE Journal 49, 1076–1084.

Kansal, I., Goel, A., Tulyaganov, D.U., Santos, L.F., Ferreira, J.M.F., 2011. Structure, surface reactivity and physico-chemical degradation of fluoride containing phosphor-silicate glasses. Journal of Materials Chemistry 21, 8074.

Kralj, D., Vdović, N., 2000. The influence of some naturally occurring minerals on the precipitation of calcium carbonate polymorphs. Water Research 34 (1), 179–184.

Li, Tie-Qiang, Häggkvist, Mats, Ödberg, Lars, 1999. The porous structure of paper coatings studied by water diffusion measurements. Colloids and Surfaces A: Physicochemical and Engineering Aspects 159, 57–63.

Malti, W.E., Laurencin, D., Guerrero, G., Smith, M.E., Mutin, P.H., 2012. Surface modification of calcium carbonate with phosphonic acids. Journal of Materials Chemistry 22, 1212.

Meiboom, S., Gill, D., 1958. Modified spin echo method for measuring nuclear relaxation times. The Review of Scientific Instruments 29, 688.

Mitchell, J., Johns, M.L., 2009. Rapid measurements of diffusion using PFG: developments and applications of the difftrain pulse sequence. Concepts in Magnetic Resonance 34A (1), 1–15.

Mitchell, J., Sederman, A.J., Fordham, E.J., Johns, M.L., Gladden, L.F., 2008a. A rapid measurement of flow propagators in porous rocks. Journal of Magnetic Resonance 191, 267–272.

Mitchell, J., von der Schulenburg, D.A., Holland, D.J., Fordham, E.J., Johns, M.L., Gladden, L.F., 2008b. Determining NMR flow propagators moments in porous rocks without the influence of relaxation. Journal of Magnetic Resonance 193, 218–225.

Mitchell, J., Chandrasekera, T.C., Johns, M.L., Gladden, L.F., Fordham, E.J., 2010. Nuclear magnetic resonance relaxation and diffusion in the presence of internal gradients: the effect of magnetic field strength. Physical Review E 81, 026101.

Petrich, C.R., Stormo, K.E., Ralston, D.R., Crawford, R.L., 1998. Encapsulated cell bioremediation: evaluation on the basis of particle tracer tests. Ground Water 36 (5), 771–778.

Phillips, B.L., Lee, Y.J., Reeder, R.J., 2005. Organic coprecipitates with calcite: NMR spectroscopic evidence. Environmental Science and Technology 39, 4533–4539.

Reggi, M.D., Gharib, B., Patard, L., Stoven, V., 1998. Lithostathine, the presumed pancreatic stone inhibitor, does not interact specifically with calcium carbonate crystals. The Journal of Biological Chemistry 273 (9), 4967–4971.

Renaudin, G., Bertrand, A., Dubois, M., Gomes, S., Chevalier, P., Labrosse, A., 2008. A study of water releases in ground (GCC) and precipitated (PCC) calcium carbonates. Journal of Physics and Chemistry of Solids 69, 1603–1614.

Scheven, U.M., Seland, J.G., Cory, D.G., 2005a. NMR-propagator measurements in porous media in the presence of surface relaxation and internal fields. Magnetic Resonance Imaging 23, 363–365.

Scheven, U.M., Verganelaskis, D., Harris, R., Johns, M.L., Gladden, L.F., 2005b. Quantitative nuclear magnetic resonance measurements of preasymptotic dispersion in flow through porous media. Physics of Fluids 17, 117107.

Sederman, A.J., Alexander, P., Gladden, L.F., 2001. Structure of packed beds probed by magnetic resonance imaging. Powder Technology 117 (3), 255–269.

Seymour, J.D., Gage, J.P., Codd, S.L., Gerlach, R., 2004. Anomalous fluid transport in porous media induced by biofilm growth. Physical Review Letters 93 (19), 198103.

Shook, G.M., Ansley, S.L., Wylie, A., 2004. Tracers and Tracer Testing: Design, Implementation, and Interpretation Methods. U.S. Dept. of Commerce (Report number: INEEL/EXT-03-01466).

Stejskal, E.O., Tanner, J.E., 1965. Spin measurements: spin echoes in the presence of a time-dependent field gradient. The Journal of Chemical Physics 42 (1), 288–292.

Tessier, J.J., Packer, K.J., 1998. The characterization of multiphase fluid transport in a porous solid by pulsed gradient stimulated echo nuclear magnetic resonance. Physics of Fluids 10 (1), 75–85.

Tobler, D.J., Cuthbert, M.O., Greswell, R.B., Riley, M.S., Renshaw, J.C., Handley-Sidhu, S., Phoenix, V.R., 2011. Comparison of rates of ureolysis between *Sporosarcina pasteurii* and an indigenous groundwater community under conditions required to precipitate large volumes of calcite. Geochimica et Cosmochimica Acta 75 (11), 3290–3301.

Tobler, D.J., Maclachlan, E., Phoenix, V.R., 2012. Microbially mediated plugging of porous media and the impact of differing injection strategies. Ecological Engineering 42, 270–278.

Verganelakis, D.A., Crawshaw, J., Johns, M.L., Mantle, M.D., Scheven, U., Sederman, A.J., Gladden, L.F., 2005. Displacement propagators of brine flowing within different types of sedimentary rock. Magnetic Resonance Imaging 23, 349–351.

Vold, R.L., Waugh, J.S., Klein, M.P., Phelps, D.E., 1968. Measurement of spin relaxation in complex systems. The Journal of Chemical Physics 48, 3831.

von der Schulenburg, D.A., Akpa, B.S., Gladden, L.F., Johns, M.L., 2008. Non-invasive mass transfer measurements in complex biofilm-coated structure. Biotechnology and Bioengineering 101, 602–608.

Warren, L.A., Maurice, P.A., Parmer, N., Ferris, F.G., 2001. Microbially mediated calcium carbonate precipitation: implications for interpreting calcite precipitation and for solid phase capture of inorganic contaminants. Geomicrobiology Journal 18, 93–115.

Whiffin, V.S., van Paassen, L.A., Harkes, M.P., 2007. Microbial carbonate precipitation as a soil improvement technique. Journal of Geomicrobiology 24, 417–423.

White, C.M., Strazisar, B.R., Granite, E.J., Hoffman, J.S., Pennline, H.W., 2003. Separation and capture of CO2 from large stationary sources and sequestration in geological formations-coalbeds and deep saline aquifers. Journal of the Air & Waste Management Association (1995) 53, 645–715.